AJR FOCUS ON:

What You Need to Know Before Reading Multiparametric MRI for Prostate Cancer

Stephanie M. Walker[1]
Peter L. Choyke
Baris Turkbey

OBJECTIVE. Multiparametric MRI (mpMRI) has become the main imaging modality for the detection, localization, and local staging of prostate cancer over the past decade. For radiologists to achieve consistent and reproducible reporting of prostate mpMRI, a comprehensive evaluation of the gland including detailed knowledge of anatomy, pathology, and clinical data is required. This article familiarizes radiologists with common pitfalls and conditions that affect mpMRI performance during readouts.

CONCLUSION. Consistent, accurate, and reproducible reporting of prostate mpMRI is vital. Additionally, radiologists should be aware of common diagnostic pitfalls that can hinder mpMRI performance.

Over the past decade, multiparametric MRI (mpMRI) has played an increasing role in prostate cancer imaging, including tumor detection, tumor characterization, risk stratification, local staging, and image guidance for biopsy and focal therapy. The ability of mpMRI to depict lesions at risk for clinically significant prostate cancer and subsequently to guide biopsies makes it an attractive alternative to random biopsies [1]. The fusion of MR images to transrectal ultrasound (TRUS) images allows MRI-directed biopsies to be performed outside the MRI suite under TRUS guidance [2].

Investigators estimated that prostate cancer would cause the death of 31,620 people in the United States in 2019 [3]. For patients with an elevated prostate-specific antigen (PSA) value or positive finding on digital rectal examination, the current standard of care is to sample the prostate with 12 systematically placed needles under TRUS guidance. Because as many as half of all prostate tumors are not visible on ultrasound, there is a significant undersampling of the prostate with this method [4]. At the same time, this method tends to overdiagnose clinically indolent prostate cancer. The latter can result in unnecessary radical treatments with consequent life-altering side effects [2].

MRI is capable of detecting clinically significant prostate cancer, but the findings tend to be nonspecific. Therefore, it is important that lesions on MRI are prioritized for biopsy. The main method used to stratify the risk of prostate lesions and select them for biopsy is the Prostate Imaging Reporting and Data System (PI-RADS), the most recent version of which was released in March 2019 [5]. This document is intended to standardize the interpretation and reporting process and increase the consistency of prostate imaging interpretations among radiologists. However, as with many subjective scales of severity, a high degree of variability exists among radiologists' prostate mpMRI interpretations, with low-to-moderate interreader agreement and intrareader agreement [6, 7].

There are several reasons why there is variability among radiologists. The prostate is a small complex organ, which makes image quality of utmost importance. Furthermore, prostate cancer varies greatly in its aggressiveness. It can be multifocal, and clinically significant tumors can be very small. The prostate has several normal anatomic components that can mimic tumor on mpMRI. Additionally, there are benign conditions, such as prostatitis and benign prostatic hyperplasia (BPH), that can obscure clinically significant tumors and make them difficult to find if the radiologist is not familiar with the pitfalls of mpMRI.

The lack of consistency among interpretations can result in unnecessary biopsies or delayed diagnosis of prostate cancer. Despite ongoing efforts by the PI-RADS Steer-

Keywords: pitfalls, Prostate Imaging Reporting and Data System (PI-RADS), prostate MRI

doi.org/10.2214/AJR.19.22751

Received December 26, 2019; accepted without revision December 26, 2019.

The opinions and assertions contained herein are the private views of the authors and are not to be construed as official or as representing the views of the National Cancer Institute or the National Institutes of Health.

Supported by the National Institutes of Health (NIH) Medical Research Scholars Program.

[1]All authors: Molecular Imaging Program, National Cancer Institute, National Institutes of Health, 10 Center Dr, Rm B3B85, Bethesda, MD 20892. Address correspondence to B. Turkbey (turkbeyi@mail.nih.gov).

This article is available for credit.

AJR 2020; 214:1211–1219

ISSN-L 0361–803X/20/2146–1211

ing Committee to standardize and simplify the reporting process, widespread education about how to interpret mpMRI of the prostate may be the most promising immediate solution. Here, we briefly discuss the classic appearance of cancers on mpMRI. We will then shed light on some of the hidden lesions and pitfalls that radiologists should be aware of before reading an mpMRI examination of the prostate as well as patient factors that can interfere with mpMRI interpretation.

The Classic Appearance of Prostate Cancer

The classic prostate cancer appears as a hypointense focus on T2-weighted imaging and on the apparent diffusion coefficient (ADC) map and as a hyperintense focus on high-b-value (> 1400 s/mm^2) imaging and shows recognizable early focal enhancement on dynamic contrast-enhanced MRI (DCE-MRI) (Fig. 1). Given that prostate cancer has a wide range of aggressiveness and presentation on mpMRI, the PI-RADS criteria set forth a framework for assigning scores on the basis of each of these individual sequences and then using these scores to derive an overall assessment category that is intended to represent the lesion's cancer risk [5]. In general, if a lesion shows positive findings on some but not all MRI sequences, its risk of cancer is considered to be lower. Conversely, larger size is associated with an increased cancer risk and is used to upgrade lesions from PI-RADS category 4 to category 5. The relationship of the lesion to the prostatic capsule is also important. If there is any evidence of extraprostatic extension (EPE) (e.g., capsular bulge, large lesion-capsule contact length, and so on), the lesion—regardless of its size—is automatically assigned the highest PI-RADS score (PI-RADS 5).

Conditions That Can Hinder Multiparametric MRI Performance

Inflammation

Inflammation in the prostate gland, as well as postinflammatory scarring, can mimic tumors on MRI. Inflammation can be caused by acute or chronic bacterial prostatitis and may be asymptomatic. Prostatitis is a common condition with a prevalence of more than 8%; prostatitis, like cancer, can result in an increase in serum PSA value and prostate volume [8]. Prostatitis causes heterogeneous background signal intensity within the prostate on T2-weighted imaging and therefore can easily lower the sensitivity and specificity of MRI for cancer detection [9] (Fig. 2). Certain findings on MRI have been shown to support a diagnosis of prostatitis, including wedge-shaped lesions, early nonfocal contrast enhancement, the absence of mass effect, and preservation of capsule integrity. However, all these findings can be present in a peripheral zone (PZ) cancer; thus, a biopsy may be the only way to definitively diagnose cancer in this setting.

Although there are many overlapping characteristics between prostatic inflammation and prostate cancer, studies support the concept that the two can be differentiated in many patients using quantitative metrics. Peker et al. [10], for example, showed that normal T2 signal intensity (mean, 3.8 vs 3.2; $p = 0.003$) and ADC values (mean, 0.685×10^{-3} mm^2/s vs 0.874×10^{-3} mm^2/s; $p < 0.001$) were significantly higher in prostatitis than in prostate cancer.

Granulomatous prostatitis is a unique inflammatory condition that may be idiopathic or a result of prior intravesical bacille Calmette-Guérin (BCG) therapy for bladder cancer, tuberculous prostatitis, or prior transurethral resection of the prostate [11]. Like cancer, granulomatous prostatitis presents clinically with elevated PSA value and a firm nodule on digital rectal examination. Although granulomatous prostatitis lesions are benign, they can present with low T2 and ADC values similar to those reported for aggressive cancers [12]. Granulomatous prostatitis nodules can also disrupt the integrity of the anatomic capsule, thus mimicking invasive cancer. In fact, a study of 16 patients with granulomatous prostatitis reported that lesions were typically scored as 5 on the PI-RADS version 2 (PI-RADSv2) scale, indicating a high suspicion for prostate cancer [11]. Because imaging features of granulomatous prostatitis can easily overlap with the imaging features of cancer-positive PI-RADS category 4 or 5 lesions, histopathologic analysis is currently regarded as the only way to definitively exclude the presence of tumor; however, a suggestive history, such as a history of BCG injection, should always be considered. Because patients with BCG-related prostatitis should be treated with isoniazid and rifampin, histologic confirmation should always be obtained [13].

Biopsy-Related Residual Hemorrhage

Hemorrhage as a result of prior biopsy will show as hyperintensity on T1-weighted images and is commonly seen in the PZ after prostate biopsy [14]. If there is a large amount of residual hemorrhage in the prostate, particularly in the PZ, the T2-weighted images can be difficult to interpret because blood products can obscure tumors. Hemorrhagic changes are low in T2 signal intensity in up to 80% of cases [15]. However, a T1-weighted test sequence can be performed in patients with a recent biopsy to screen for the presence of hemorrhage before completing the T2-weighted, DW, and DCE-MRI sequences to save the patient time and IV contrast medium exposure and to avoid the need for a repeat study. Postbiopsy hemorrhage can persist for months, but the MRI changes resolve over time, and an interval of at least 6 weeks is recommended between biopsy and MRI [16].

Although the presence of hemorrhage worsens the quality of the T2-weighted sequence, the T1-weighted sequence in patients with hemorrhage can reveal a possible tumor in some cases. Compared with normal prostate tissue, cancers have reduced levels of citrate, which acts as an anticoagulant and promotes the resolution of hemorrhage faster than healthy tissue. This finding is referred to as the "hemorrhage exclusion" sign and is defined as T1-weighted images showing a hyperintense PZ, indicating hemorrhage, except for a signal-void area, which indicates involvement by tumor [17]. The hemorrhage exclusion sign is not always diagnostic but can be supportive evidence when combined with findings on T2-weighted imaging or DWI (Fig. 3).

Presence of a Hip Prosthesis

Susceptibility artifacts due to hip prostheses are common and can limit the diagnostic accuracy of mpMRI [18]. Increasing numbers of patients with hip replacements are presenting for pelvic imaging, because more than 5% of Americans will have undergone a total hip replacement by age 80 [19]. For prostate MRI, the T2-weighted sequence is less likely to be affected because it is a spin-echo sequence, which is not prone to metallic artifacts, unlike gradient-echo pulse sequences. The gradient-echo pulse sequences such as DWI and DCE-MRI are more strongly affected by hip prostheses (Fig. 4). One potential solution is to use a lower magnetic field strength (i.e., 1.5 T) at which the susceptibility artifacts are reduced [5, 20, 21]. Additionally, the use of novel acquisition techniques, such as periodically rotated overlapping parallel lines with enhanced reconstruction or reduced-FOV DWI, can aid ac-

quisition of diagnostic DWI in patients with a hip prosthesis [20, 22].

Presence of Rectal Gas-Related Susceptibility Artifacts

Rectal gas has been reported to diminish the quality and accuracy of DWI by causing significant susceptibility artifacts. The presence of rectal gas affects echo-planar imaging (EPI) pulse sequences, which are used for DWI acquisition [23]. Susceptibility artifacts commonly occur at soft tissue–air interfaces (PZ of the prostate and rectal lumen) and lesions that are suspicious for prostate cancer can be easily missed. Although there is not an established and proven method to avoid rectal gas-related susceptibility artifacts, some methods have been proposed in the literature, such as asking the patient to empty the bowel before MRI acquisition, use of antispasmodic agents, bowel cleaning using enema, evacuation of rectal gas via a thin catheter, or prone positioning for imaging [24]. Additionally, there are a limited number of image acquisition and postprocessing techniques such as reduced-FOV DWI, parallel imaging, shortened EPI, turbo spin-echo readout, and correction for B_0 distortion [20, 22, 24, 25]. Although some of these approaches have shown benefit, more research is needed to understand their actual benefit. When a rectal gas-related susceptibility artifact on DWI is encountered during prostate MRI readout, careful evaluation of T2-weighted imaging and DCE-MRI becomes crucial. If the study is not diagnostic, repeat prostate MRI using one of the preparation methods mentioned earlier can be considered.

Effects of Prior Treatments

Although radical prostatectomy is the most commonly used approach for the treatment of localized prostate cancer, several other methods such as focal treatment (e.g., laser ablation, cryoablation), radiation therapy, and androgen deprivation therapy (ADT) are also used in the management of localized disease. After successful focal therapy, the treated lesions are typically diffusely hypointense and have a bandlike shape on T2-weighted images and ADC maps, and DCE-MR images show a lack of focal enhancement (Fig. 5). When tumors recur after focal therapy, their appearance is similar to treatment-naïve cancers with hypointense signal on T2-weighted images and ADC maps, hyperintense signal on high-b-value DW images, and focal early enhancement on DCE-MR images [26].

After radiotherapy, the entire prostate gland often appears diffusely heterogeneous with considerable amounts of low-level background signal intensity, making it challenging to detect recurrent disease foci. Recurrent or residual disease can appear hypointense on T2-weighted MRI and ADC maps and can show focal enhancement on DCE-MRI (Fig. 6). It is helpful to check the seminal vesicles in patients with a history of radiation [27, 28].

ADT has been shown to be effective for controlling both local and distant castration-sensitive tumors in neoadjuvant, adjuvant, and recurrence settings [29–32]. ADT is known to significantly decrease prostate volume and PSA values. ADT has been shown to affect MRI tumor characteristics such as ADC and K^{trans} values. Hötker et al. [33] revealed that ADC values increased by an average of 17% and K^{trans} values decreased by up to 56% in tumors treated with ADT. Padhani et al. [34] also reported a decrease in vascular permeability within tumors and the gland as a whole after ADT. Additionally, ADT reduced the signal intensity of the PZ, which reduced tumor-PZ contrast [34]. ADT commonly results in a diffuse heterogeneous signal intensity on T2-weighted images, DW images, and ADC maps and a diffuse patchy enhancement pattern on DCE-MR images. These changes, in addition to an atrophic gland, can easily mask visualization of residual or recurrent cancer foci.

Although interpretation of posttreatment mpMRI is challenging, evaluation of posttreatment mpMRI can nevertheless provide localization of a recurrent tumor [35]. A key step in identifying recurrence is documenting the initial location of the disease before treatment because recurrences are most likely at or near the initial tumor [26]. Finally, PI-RADS categories cannot be used in patients who have received ADT because PI-RADS applies only to treatment-naïve patients.

Pitfalls During Prostate MRI Evaluation

Benign Prostatic Hyperplasia

BPH is one of the most frequent diagnoses in men and, because it is symptomatic, requires urologic referral. More than 80% of men develop BPH in their lifetime and as many as 30% receive treatment [36]. BPH is characterized by hyperplasia of prostatic stromal and epithelial cells, resulting in large discrete nodules within the transition zone (TZ). On MRI, BPH shows an enlarged TZ with highly variable signal-intensity characteristics based on the ratio of glandular tissue to stromal tissue [37]. BPH nodules with predominantly glandular tissue appear more hyperintense on T2-weighted images, whereas BPH nodules consisting of mostly stromal tissue appear hypointense on T2-weighted images, leading to a diagnostic dilemma [38]. In most patients with BPH, MRI shows a heterogeneous appearance in the TZ [39].

Stromal BPH nodules and TZ tumors overlap in T2, ADC, and K^{trans} values [38]. For this reason, morphology and texture of the nodules on T2-weighted images are most helpful when differentiating stromal BPH nodules in the TZ from cancerous tumor. Characteristics on T2-weighted images that support the diagnosis of cancer in the TZ include homogeneously low signal intensity (sensitivity, 76–78%; specificity, 78–87%), ill-defined margins (sensitivity, 76–78%; specificity, 78–89%), and lenticular shape (sensitivity, 48–56%; specificity, 85–98%) [40]. Invasion into adjacent structures, such as the anterior fibromuscular stroma (AFMS), anatomic capsule, or PZ, also suggests cancer. Spherical encapsulated nodules with heterogeneously low signal intensity are more likely stromal BPH than cancer [40–42]. Although quantitative approaches have been shown to be helpful to distinguish a BPH lesion from a cancer lesion, the use of current morphologic definitions, which are substantially subjective, is the recommended method for prostate MRI evaluation in the TZ.

Central Zone

The central zone (CZ) surrounds the ejaculatory ducts, is located posterior to the urethra and PZ, and is proximal to the verumontanum [43]. The CZ usually appears as bilateral and symmetric low-signal-intensity tissue on T2-weighted and ADC images and therefore can occasionally be mistaken for cancer. On high-b-value DWI, the CZ is mildly hyperintense. No early enhancement is seen on DCE-MRI in normal CZ tissue.

Although very rare, cancer can develop in the CZ and tends to be more aggressive than cancer originating in the TZ or PZ [44]. Findings that suggest normal CZ tissue are bilateral symmetry and lack of focal enhancement, whereas asymmetry between the right and left CZs on T2-weighted, ADC, or high-b-value images or focal early enhancement may suggest a CZ cancer. Most lesions appearing to be in the CZ arise in the adja-

cent TZ or PZ and extend into the CZ. Although asymmetry of the CZ could suggest cancer, it is important to note that BPH can distort the appearance of the CZ and some CZ asymmetry can be considered normal variation. Moreover, if the plane of section is not truly parallel to the long axis of the prostate, the CZ can appear asymmetric [45] (Fig. 7).

Anterior Fibromuscular Stroma

The normal prostate gland includes the AFMS. The AFMS appears as an anterior symmetric crescent-shaped area with low signal intensity on T2-weighted imaging, ADC maps, and high-b-value DWI and does not show early focal enhancement on DCE-MRI. It extends from the apex to the base of the prostate and is thicker in the midline, giving it a characteristic crescent shape. A prominent stroma can easily mimic cancer; therefore, careful evaluation of the AFMS can be helpful. The AFMS decreases in size as men age, from a mean anteroposterior thickness of 1.2 cm in the 2nd decade to 0.4 cm in the 8th decade [46]. Cancer does not originate in the AFMS, but PZ and TZ lesions can extend into the AFMS and lead to suspicious-appearing areas within the AFMS. A loss of symmetry of the AFMS on mpMRI, as well as focal enhancement on DCE-MRI, should raise suspicion for prostate cancer extending into the AFMS [45]. Anterior tumors in the prostate account for approximately 21% of prostate cancers and are usually not palpable on digital rectal examination [47]. Anterior tumors are associated with higher PSA levels and have higher rates of EPE at surgery than posterior tumors and therefore should be carefully investigated on imaging [48, 49].

Periprostatic Venous Plexus

The periprostatic venous plexus, also known as the Santorini plexus, is located circumferentially along each side of the prostate and ultimately drains into the internal iliac veins [50]. The size of these veins varies greatly among patients and decreases with patient age [46]. In older patients with enlarged prostates, the venous plexus is not always visualized, probably because of stretching and effacement of the vessels [51]. The periprostatic venous plexus runs closely along the anatomic capsule of the prostate and may actually be embedded within it at some points along its course [52]. Distortion or obliteration of the venous plexus on imaging can indicate tumor extension beyond the capsule.

On MRI, veins are typically hyperintense tubular structures on T2-weighted imaging; however, the signal intensity varies with velocity and turbulence of the blood flow [39]. Periprostatic veins, especially the prominent ones, with lower signal intensity on T2-weighted images and ADC maps can mimic cancer. They enhance avidly on DCE-MRI with a linear morphology. Careful examination of these tubular, linear structures in all planes will help show continuity with the rest of the venous plexus.

Thickened Surgical Capsule

The prostate is contained within an anatomic capsule that surrounds the PZ. Radiologists are familiar with this capsule because it serves as a key landmark for assessing local EPE and is required for treatment planning. A so-called surgical capsule is separate from the anatomic capsule and exists between the TZ and PZ in patients with BPH [53]. In this population, the surgical capsule typically varies from 2 to 5 mm and consists of a thickened fibromuscular layer. The outward pressure from BPH growth in the TZ results in proliferation of the surgical capsule. The surgical capsule is so named because it serves as a key landmark for the intended treatment volume during surgical enucleation of the TZ to treat symptoms of BPH [54, 55].

On T2-weighted MRI, the surgical capsule appears hypointense and surrounds the TZ. It is also hypointense on ADC maps. There is variation among the appearance of the surgical capsule, because BPH patterns vary greatly and may cause asymmetric thickening. With a hypointense appearance on both T2-weighted images and ADC maps, the surgical capsule may raise suspicion for cancer. Detailed knowledge of this normal anatomic feature is helpful in differentiating the surgical capsule from cancer. Correlating the ADC maps with the T2-weighted images when these lesions are noted surrounding the TZ, especially when symmetry is present, should support the finding of a normal surgical capsule and should lower suspicion for cancer [56].

Pseudolesions of the Posterior Midline Peripheral Zone

In some patients, the posterior midline of the PZ of the prostate can show a homogeneous hypointense midline signal intensity on T2-weighted MRI and corresponding hypointense signal features on ADC maps, hyperintense signal features on high-b-value DW images, and early focal enhancement on DCE-MR images. The exact cause of this commonly encountered pitfall is not clear, but a few studies have shown that the posterior midline of the PZ of the prostate corresponds to the fusion of the prostate capsule and overlying fascia at the junction of the two prostatic lobes [57]. Although it may be difficult to distinguish this pseudolesion appearance from a real tumor, if the area showing abnormal signal intensity is more rounded with a masslike shape on T2-weighted MR images and ADC maps and shows early focal enhancement on DCE-MR images, the radiologist must be alerted about a lesion suspicious for prostate cancer located in the posterior midline of the PZ [58] (Fig. 5).

Conclusion

Prostate mpMRI is increasingly being used for tumor localization in the prostate because mpMRI can be used to guide targeted biopsies to improve the detection of prostate cancer. However, some challenges in making an accurate diagnosis remain. Consistent, accurate, and reproducible reporting of prostate mpMRI examinations is vital. Additionally, radiologists should be aware of common diagnostic pitfalls that can hinder mpMRI performance. In this article, we have covered some key aspects of what radiologists should know before reading mpMRI studies of the prostate.

References

1. Oberlin DT, Casalino DD, Miller FH, Meeks JJ. Dramatic increase in the utilization of multiparametric magnetic resonance imaging for detection and management of prostate cancer. *Abdom Radiol (NY)* 2017; 42:1255–1258
2. Ahmed HU, El-Shater Bosaily A, Brown LC, et al.; PROMIS Study Group. Diagnostic accuracy of multi-parametric MRI and TRUS biopsy in prostate cancer (PROMIS): a paired validating confirmatory study. *Lancet* 2017; 389:815–822
3. Siegel RL, Miller KD, Jemal A. Cancer statistics, 2019. *CA Cancer J Clin* 2019; 69:7–34
4. Halpern EJ, Strup SE. Using gray-scale and color and power Doppler sonography to detect prostatic cancer. *AJR* 2000; 174:623–627
5. Turkbey B, Rosenkrantz AB, Haider MA, et al. Prostate Imaging Reporting and Data System Version 2.1: 2019 update of Prostate Imaging Reporting and Data System Version 2. *Eur Urol* 2019; 76:340–351
6. Smith CP, Harmon SA, Barrett T, et al. Intra- and interreader reproducibility of PI-RADSv2: a multireader study. *J Magn Reson Imaging* 2019; 49:1694–1703

7. Ke Z, Wang L, Min XD, et al. Diagnostic performance and interobserver consistency of the Prostate Imaging Reporting and Data System Version 2: a study on six prostate radiologists with different experiences from half a year to 17 years. *Chin Med J (Engl)* 2018; 131:1666–1673
8. Krieger JN, Lee SW, Jeon J, Cheah PY, Liong ML, Riley DE. Epidemiology of prostatitis. *Int J Antimicrob Agents* 2008; 31(suppl 1):S85–S90
9. Hötker AM, Dappa E, Mazaheri Y, et al. The influence of background signal intensity changes on cancer detection in prostate MRI. *AJR* 2019; 212:823–829
10. Peker E, Sonmez DY, Akkaya HE, Hayme S, Erden MI, Erden A. Diagnostic performance of multiparametric MR imaging at 3.0 tesla in discriminating prostate cancer from prostatitis: a histopathologic correlation. *Eurasian J Med* 2019; 51:31–37
11. Lee SM, Wolfe K, Acher P, Liyanage SH. Multiparametric MRI appearances of primary granulomatous prostatitis. *Br J Radiol* 2019; 92:20180075
12. Yu AC, Badve C, Ponsky LE, et al. Development of a combined MR fingerprinting and diffusion examination for prostate cancer. *Radiology* 2017; 283:729–738
13. Rischmann P, Desgrandchamps F, Malavaud B, Chopin DK. BCG intravesical instillations: recommendations for side-effects management. *Eur Urol* 2000; 37(suppl 1):33–36
14. Lovegrove CE, Matanhelia M, Randeva J, et al. Prostate imaging features that indicate benign or malignant pathology on biopsy. *Transl Androl Urol* 2018; 7(suppl 4):S420–S435
15. Kaji Y, Kurhanewicz J, Hricak H, et al. Localizing prostate cancer in the presence of postbiopsy changes on MR images: role of proton MR spectroscopic imaging. *Radiology* 1998; 206:785–790
16. Weinreb JC, Barentsz JO, Choyke PL, et al. PI-RADS Prostate Imaging – Reporting and Data System: 2015, Version 2. *Eur Urol* 2016; 69:16–40
17. Purysko AS, Herts BR. Prostate MRI: the hemorrhage exclusion sign. *J Urol* 2012; 188:1946–1947
18. Lüdeke KM, Röschmann P, Tischler R. Susceptibility artefacts in NMR imaging. *Magn Reson Imaging* 1985; 3:329–343
19. Maradit Kremers H, Larson DR, Crowson CS, et al. Prevalence of total hip and knee replacement in the United States. *J Bone Joint Surg Am* 2015; 97:1386–1397
20. Czarniecki M, Caglic I, Grist JT, et al. Role of PROPELLER-DWI of the prostate in reducing distortion and artefact from total hip replacement metalwork. *Eur J Radiol* 2018; 102:213–219
21. Campbell-Washburn AE, Ramasawmy R, Restivo MC, et al. Opportunities in interventional and diagnostic imaging by using high-performance low-field-strength MRI. *Radiology* 2019; 293:384–393
22. Rosenkrantz AB, Taneja SS. Use of reduced field-of-view acquisition to improve prostate cancer visualization on diffusion-weighted magnetic resonance imaging in the presence of hip implants: report of 2 cases. *Curr Probl Diagn Radiol* 2018; 47:125–127
23. Caglic I, Hansen NL, Slough RA, Patterson AJ, Barrett T. Evaluating the effect of rectal distension on prostate multiparametric MRI image quality. *Eur J Radiol* 2017; 90:174–180
24. Caglic I, Barrett T. Optimising prostate mpMRI: prepare for success. *Clin Radiol* 2019; 74:831–840
25. Jambor I. Optimization of prostate MRI acquisition and post-processing protocol: a pictorial review with access to acquisition protocols. *Acta Radiol Open* 2017; 6:2058460117745574
26. Patel P, Mathew MS, Trilisky I, Oto A. Multiparametric MR imaging of the prostate after treatment of prostate cancer. *RadioGraphics* 2018; 38:437–449
27. Mertan FV, Greer MD, Borofsky S, et al. Multiparametric magnetic resonance imaging of recurrent prostate cancer. *Top Magn Reson Imaging* 2016; 25:139–147
28. Valle LF, Greer MD, Shih JH, et al. Multiparametric MRI for the detection of local recurrence of prostate cancer in the setting of biochemical recurrence after low dose rate brachytherapy. *Diagn Interv Radiol* 2018; 24:46–53
29. McKay RR, Ye H, Xie W, et al. Evaluation of intense androgen deprivation before prostatectomy: a randomized phase II trial of enzalutamide and leuprolide with or without abiraterone. *J Clin Oncol* 2019; 37:923–931
30. Gamat M, McNeel DG. Androgen deprivation and immunotherapy for the treatment of prostate cancer. *Endocr Relat Cancer* 2017; 24:T297–T310
31. Sharifi N, Gulley JL, Dahut WL. Androgen deprivation therapy for prostate cancer. *JAMA* 2005; 294:238–244
32. Sharifi N, Gulley JL, Dahut WL. An update on androgen deprivation therapy for prostate cancer. *Endocr Relat Cancer* 2010; 17:R305–R315
33. Hötker AM, Mazaheri Y, Zheng J, et al. Prostate cancer: assessing the effects of androgen-deprivation therapy using quantitative diffusion-weighted and dynamic contrast-enhanced MRI. *Eur Radiol* 2015; 25:2665–2672
34. Padhani AR, MacVicar AD, Gapinski CJ, et al. Effects of androgen deprivation on prostatic morphology and vascular permeability evaluated with MR imaging. *Radiology* 2001; 218:365–374
35. Fennessy FM, Fedorov A, Vangel MG, et al. Multiparametric MRI as a biomarker of response to neoadjuvant therapy for localized prostate cancer: a pilot study. *Acad Radiol* 2019 Dec 17 [Epub ahead of print]
36. Grossfeld GD, Coakley FV. Benign prostatic hyperplasia: clinical overview and value of diagnostic imaging. *Radiol Clin North Am* 2000; 38:31–47
37. Kirby RS. The clinical assessment of benign prostatic hyperplasia. *Cancer* 1992; 70(suppl):284–290
38. Oto A, Kayhan A, Jiang Y, et al. Prostate cancer: differentiation of central gland cancer from benign prostatic hyperplasia by using diffusion-weighted and dynamic contrast-enhanced MR imaging. *Radiology* 2010; 257:715–723
39. Kitzing YX, Prando A, Varol C, Karczmar GS, Maclean F, Oto A. Benign conditions that mimic prostate carcinoma: MR imaging features with histopathologic correlation. *RadioGraphics* 2016; 36:162–175
40. Hoeks CMA, Hambrock T, Yakar D, et al. Transition zone prostate cancer: detection and localization with 3-T multiparametric MR imaging. *Radiology* 2013; 266:207–217
41. Li H, Sugimura K, Kaji Y, et al. Conventional MRI capabilities in the diagnosis of prostate cancer in the transition zone. *AJR* 2006; 186:729–742
42. Akin O, Sala E, Moskowitz CS, et al. Transition zone prostate cancers: features, detection, localization, and staging at endorectal MR imaging. *Radiology* 2006; 239:784–792
43. Vargas HA, Akin O, Franiel T, et al. Normal central zone of the prostate and central zone involvement by prostate cancer: clinical and MR imaging implications. *Radiology* 2012; 262:894–902
44. Cohen RJ, Shannon BA, Phillips M, Moorin RE, Wheeler TM, Garrett KL. Central zone carcinoma of the prostate gland: a distinct tumor type with poor prognostic features. *J Urol* 2008; 179:1762–1767; discussion, 1767
45. Chatterjee A, Thomas S, Oto A. Prostate MR: pitfalls and benign lesions. *Abdom Radiol (NY)* 2019 Nov 8 [Epub ahead of print]
46. Allen KS, Kressel HY, Arger PH, Pollack HM. Age-related changes of the prostate: evaluation by MR imaging. *AJR* 1989; 152:77–81
47. Bott SR, Young MP, Kellett MJ, Parkinson MC; Contributors to the UCL Hospitals' Trust Radical Prostatectomy Database. Anterior prostate cancer: is it more difficult to diagnose? *BJU Int* 2002; 89:886–889
48. Koppie TM, Bianco Jr FJ, Kuroiwa K, et al. The clinical features of anterior prostate cancers. *BJU Int* 2006; 98:1167–1171
49. Mygatt J, Sesterhenn I, Rosner I, et al. Anterior tumors of the prostate: clinicopathological features and outcomes. *Prostate Cancer Prostatic Dis* 2014; 17:75–80
50. Phillips ME, Kressel HY, Spritzer CE, et al. Normal prostate and adjacent structures: MR imaging at 1.5 T. *Radiology* 1987; 164:381–385
51. Hricak H, Dooms GC, McNeal JE, et al. MR imaging of the prostate gland: normal anatomy. *AJR* 1987; 148:51–58
52. Poon PY, Bronskill MJ, Poon CS, McCallum RW,

Bruce AW, Henkelman RM. Identification of the periprostatic venous plexus by MR imaging. *J Comput Assist Tomogr* 1991; 15:265–268

53. Semple JE. Surgical capsule of the benign enlargement of the prostate: its development and action. *BMJ* 1963; 1:1640–1643
54. Oh SJ. Current surgical techniques of enucleation in holmium laser enucleation of the prostate. *Investig Clin Urol* 2019; 60:333–342
55. Palaniappan S, Kuo TLC, Cheng CWS, Foo KT. Early outcome of transurethral enucleation and resection of the prostate versus transurethral resection of the prostate. *Singapore Med J* 2016; 57:676–680
56. Rosenkrantz AB, Taneja SS. Radiologist, be aware: ten pitfalls that confound the interpretation of multiparametric prostate MRI. *AJR* 2014; 202:109–120
57. Kiyoshima K, Yokomizo A, Yoshida T, et al. Anatomical features of periprostatic tissue and its surroundings: a histological analysis of 79 radical retropubic prostatectomy specimens. *Jpn J Clin Oncol* 2004; 34:463–468
58. Rosenkrantz AB, Verma S, Turkbey B. Prostate cancer: top places where tumors hide on multiparametric MRI. *AJR* 2015; 204:[web]W449–W456

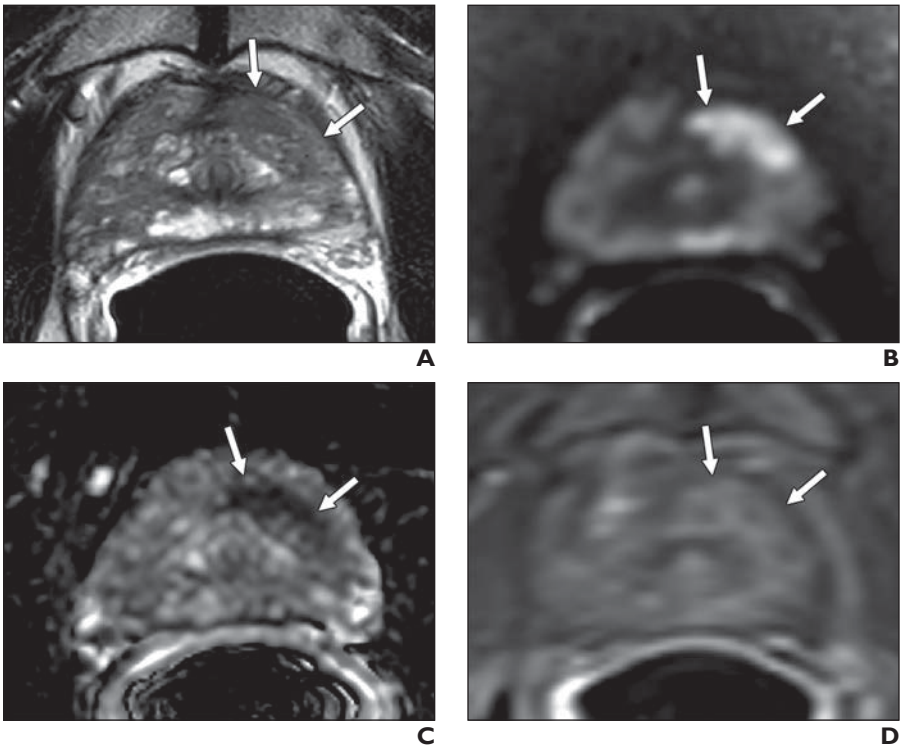

Fig. 1—67-year-old man with serum prostate-specific antigen value of 17.20 ng/mL who was referred for multiparametric MRI (mpMRI); 3-T mpMR images obtained with endorectal coil show classic Prostate Imaging Reporting and Data System (PI-RADS) 5 lesion measuring 2.4 cm in left apical–mid anterior peripheral zone.
A–D, Lesion (*arrows*) is hypointense with ill-defined borders on axial T2-weighted image (**A**), hyperintense on high-b-value DW image (**B**), hypointense on apparent diffusion coefficient map (**C**), and enhancing on dynamic contrast-enhanced MR image (**D**). Overall PI-RADS score of 5 was given to this lesion. At pathology, lesion was found to include Gleason 3 + 4 prostate cancer.

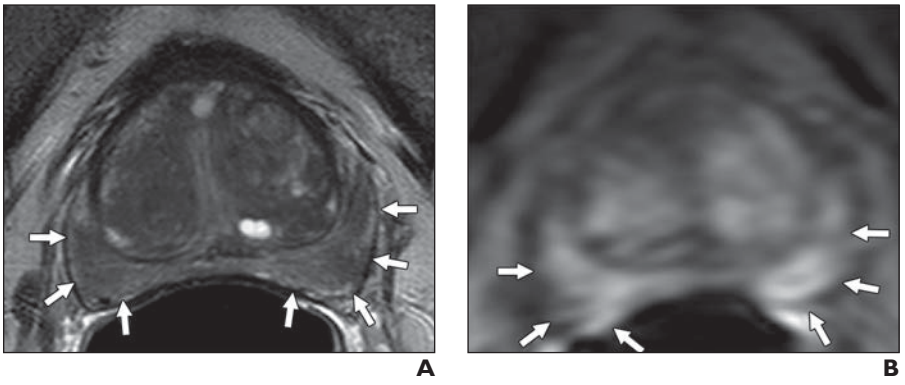

Fig. 2—57-year-old man with serum prostate-specific antigen value of 9.31 ng/mL who was referred for multiparametric MRI (mpMRI); 3-T mpMR images are shown.
A and **B,** Patchy signal pattern in peripheral zone (*arrows*, **A**) is seen on T2-weighted image (**A**), and diffuse enhancement (*arrows*, **B**) is seen on dynamic contrast-enhanced MR image (**B**). These findings suggest inflammatory process.

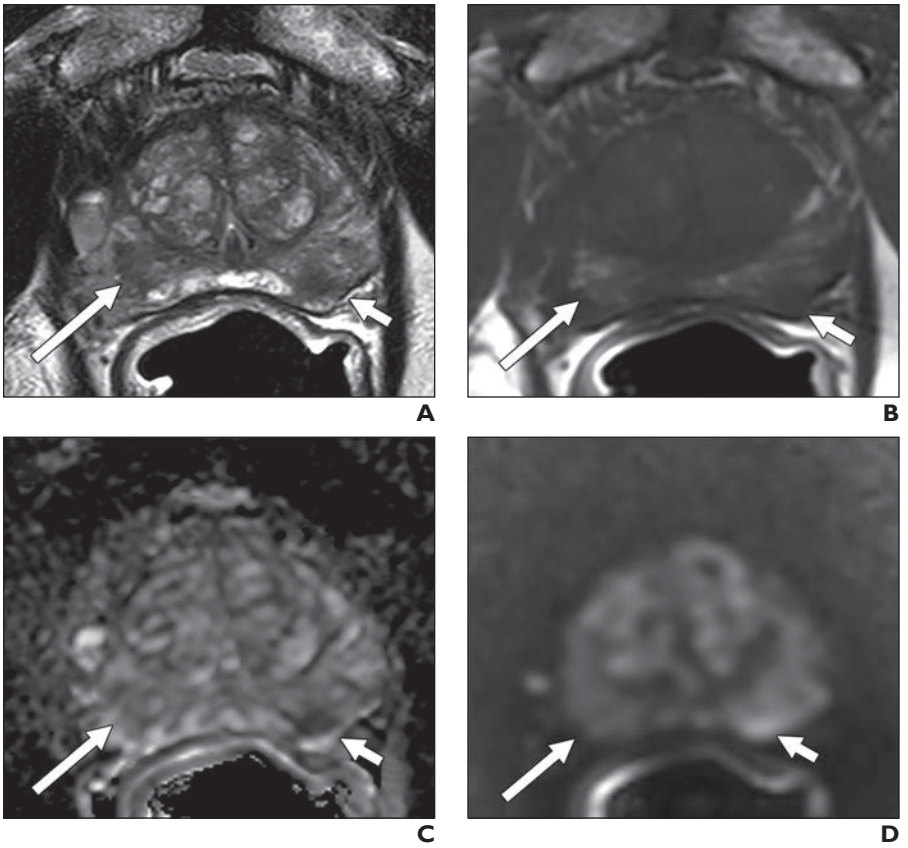

Fig. 3—77-year-old man with serum prostate-specific antigen value of 6.12 ng/mL who was referred for multiparametric MRI (mpMRI); 3-T mpMRI examination was performed with endorectal coil.
A, T2-weighted image shows right-sided (*long arrow*) and left-sided (*short arrow*) lesions along with patchy peripheral zone.
B, Axial T1-weighted image shows biopsy-related residual hemorrhage within right-sided lesion (*long arrow*) and "hemorrhage exclusion" sign within left-sided lesion (*short arrow*).
C and **D,** Apparent diffusion coefficient map (**C**) and high-b-value DW image (**D**) show hypointense and hyperintense signal features within left-sided lesion (*short arrows*) that are suspicious for prostate cancer, but signal-intensity features appear normal within right-sided lesion (*long arrows*); this difference in findings is example of potential source of false-positive lesion at T2-weighted prostate MRI secondary to biopsy-related residual hemorrhage.

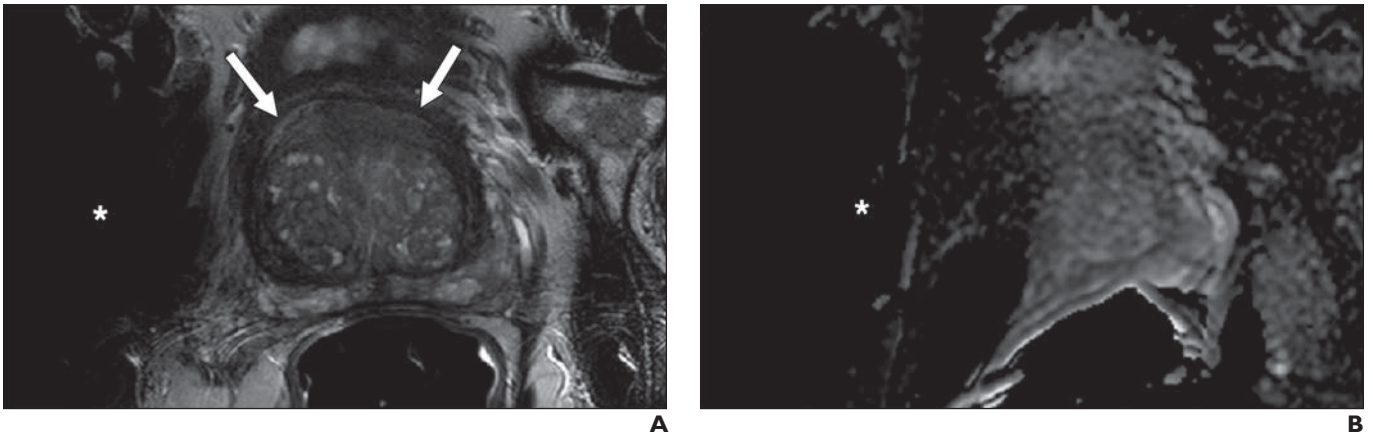

Fig. 4—63-year-old man who presented with serum prostate-specific antigen value of 42 ng/mL and history of negative results on 10 previous transrectal ultrasound–guided biopsies; 3-T multiparametric MRI examination was performed with endorectal coil.
A, T2-weighted image shows midline anterior transition zone lesion (*arrows*) despite right-sided hip prosthesis artifacts (*asterisk*).
B, Apparent diffusion coefficient map is nondiagnostic because of right-sided hip prosthesis artifacts (*asterisk*). Targeted biopsy of lesion shown in **A** revealed Gleason 4 + 5 prostate cancer.

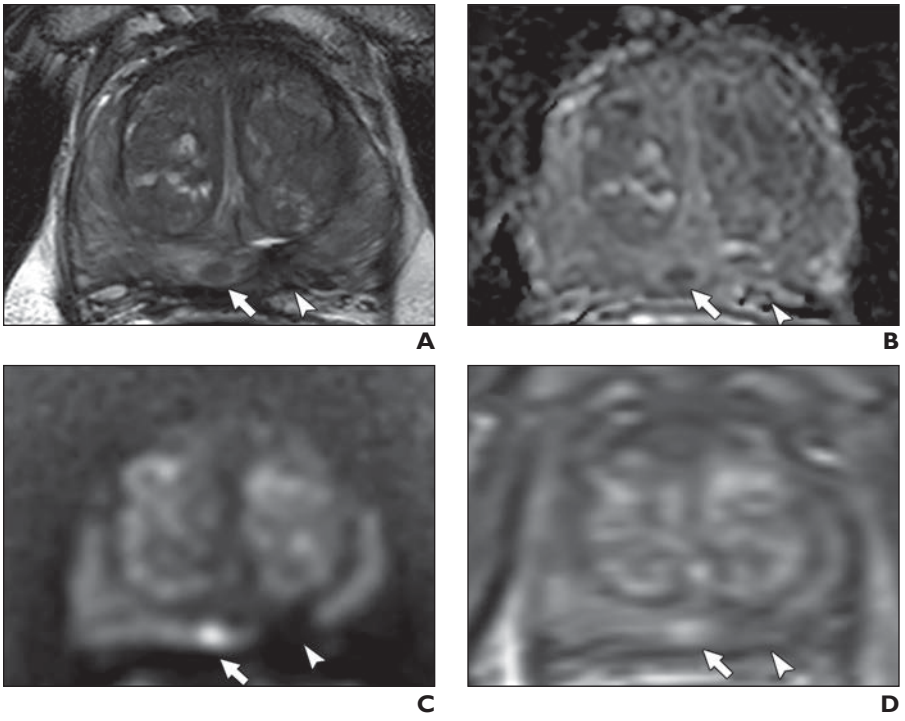

Fig. 5—69-year-old man with serum prostate-specific antigen value of 8.38 ng/mL.
A–D, Multiparametric MRI (mpMRI) shows band-shaped hypointense signal features (*arrowhead*, **A**) in left apical–mid peripheral zone on T2-weighted MR image (**A**), with signal void patterns (*arrowheads*, **B** and **C**) on apparent diffusion coefficient map (**B**) and high-b value DW image (**C**) without evidence of focal enhancement (*arrowhead*, **D**) on dynamic contrast-enhanced MR image (**D**). Findings are consistent with focal laser ablation changes within left apical–mid peripheral zone without evidence of recurrent lesion. Additional finding is seen in posterior midline apical–mid peripheral zone as round hypointense lesion (*arrow*) in **A**, with corresponding hypointense and hyperintense signal patterns (*arrows*) in **B** and **C**, respectively, with focal enhancement (*arrow*) seen in **D**. Targeted biopsy revealed Gleason 3 + 3 prostatic adenocarcinoma within this lesion.

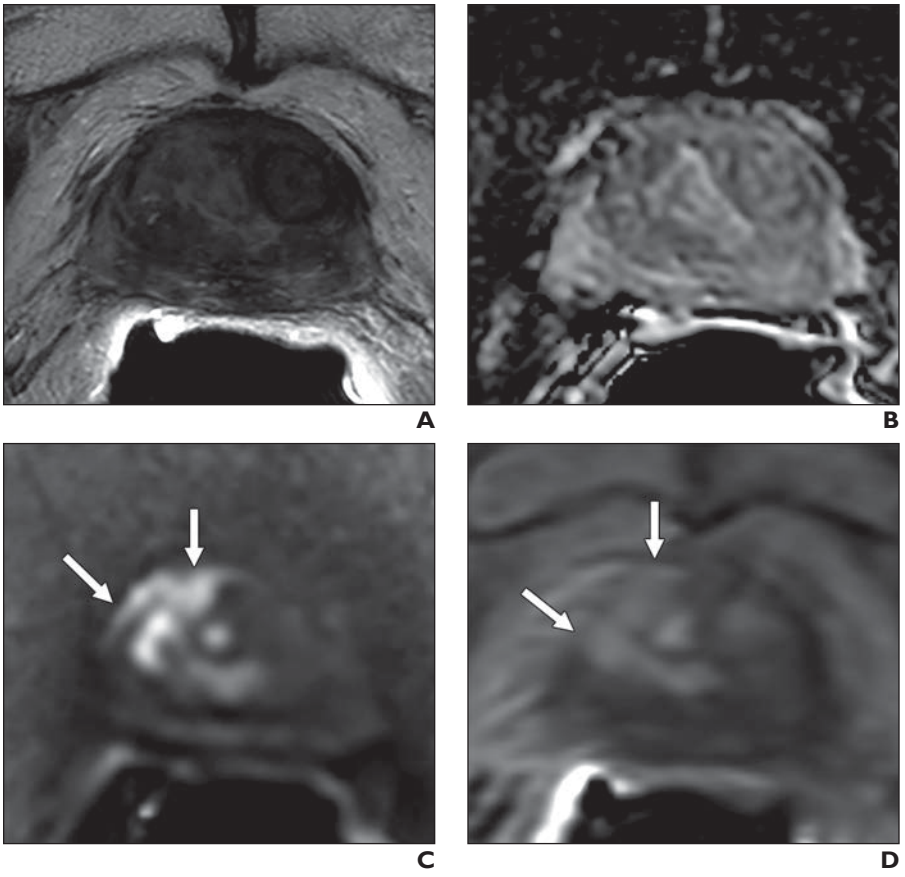

Fig. 6—82-year-old man with history of external beam radiation therapy for localized prostate cancer who presented with serum prostate-specific antigen value of 9.33 ng/mL. Patient was referred for multiparametric MRI.
A, T2-weighted image shows diffusely heterogeneous signal pattern without evidence of focal lesion.
B, Apparent diffusion coefficient map shows unremarkable findings.
C and **D,** High-b-value DW image (**C**) and dynamic contrast-enhanced MR image (**D**) show focal lesion in right mid anterior transition zone (*arrows*). Targeted biopsy revealed recurrent prostate cancer within this lesion.

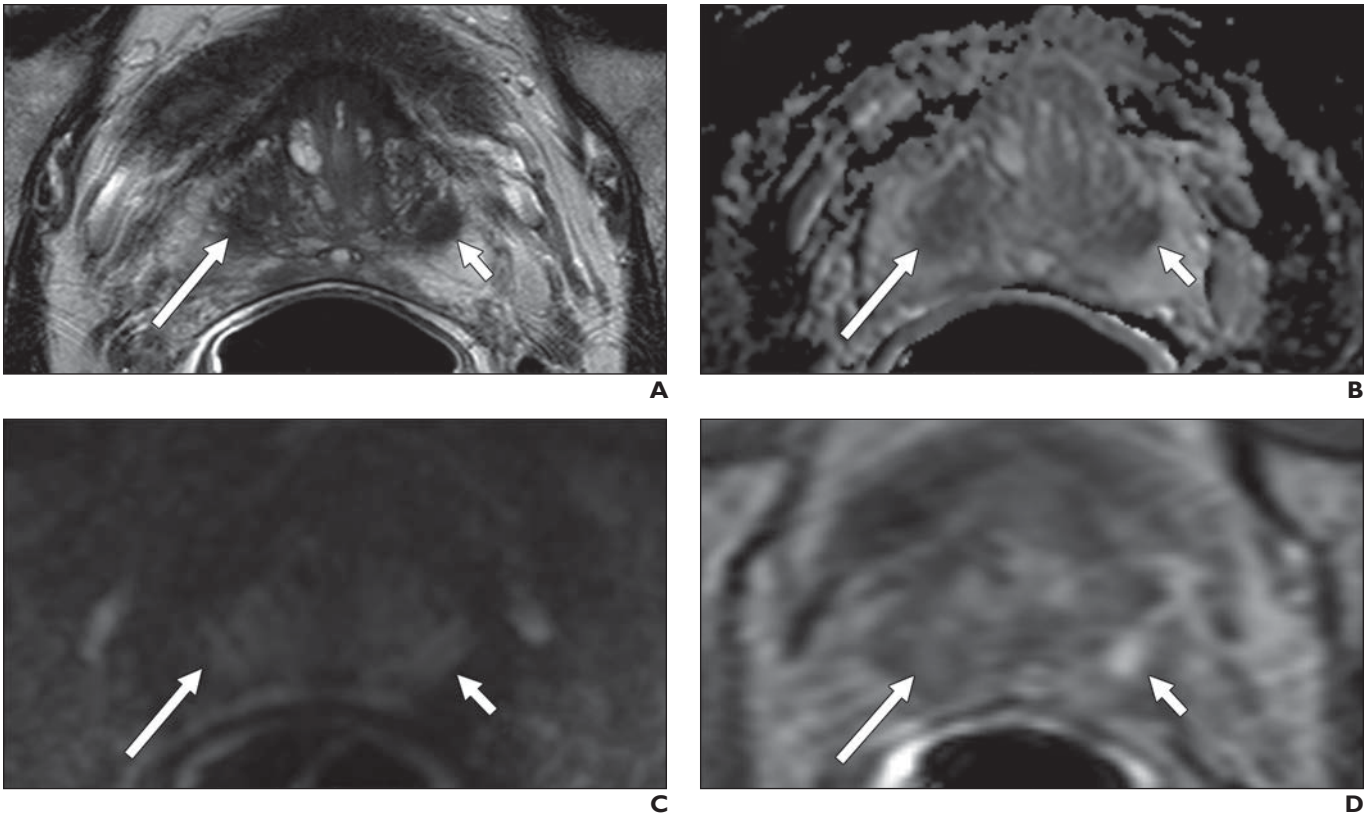

Fig. 7—62-year-old man with serum prostate-specific antigen value of 6.4 ng/mL who was referred for multiparametric MRI (mpMRI).
A, T2-weighted image shows asymmetric hypointense lesion in left central zone (CZ) (*short arrow*) compared with right CZ (*long arrow*).
B, Apparent diffusion coefficient image shows asymmetric hypointense signal in left CZ lesion (*short arrow*) compared with normal contralateral CZ (*long arrow*).
C, High-b-value DW image shows asymmetric hyperintense signal in left CZ lesion (*short arrow*) compared with normal contralateral CZ (*long arrow*).
D, Dynamic contrast-enhanced MR image shows early intense asymmetric enhancement within left CZ lesion (*short arrow*), whereas corresponding right CZ (*long arrow*) appears normal.